Princeton/HEP/93-03
May 28, 1993

Properties of Reflective and Semitransparent CsI Photocathodes

C. Lu and K.T. McDonald

Joseph Henry Laboratories, Princeton University, Princeton, NJ 08544

Abstract

Various aspects related to the quantum efficiency of the reflective and semitransparent CsI photocathodes have been investigated experimentally. The investigation explored the dependence of the quantum efficiency on the following: the thickness of the photocathode film, the gas used in the parallel-plate avalanche chamber, exposure to water vapor, and the density of the CsI film. With reflective CsI photocathodes quantum efficiencies of more than 25% at 180 nm have achieved in three different gases: CH_4, C_2H_6, and C_4H_{10}. Our study reveals that high quantum efficiency is also achievable for the semitransparent CsI photocathodes. For a 95-Å semitransparent photocathode the quantum efficiency at 185 nm can be as high as 20%. A simple model to explain the dependance of quantum efficiency on the thickness of CsI photocathodes is suggested, which may be a useful guide for further improvement of the performance of CsI photocathodes. Also reported are UV-transmittance measurements for various materials used in our studies, such as methane, ethane, isobutane, CF_4, CO_2, helium, neon, air, TMAE vapor, thin CsI films, and quartz windows, all in the wavelength range 115 nm to 230 nm.

Presented at the
First Workshop on RICH Detectors
Bari, Italy, June 2-5, 1993

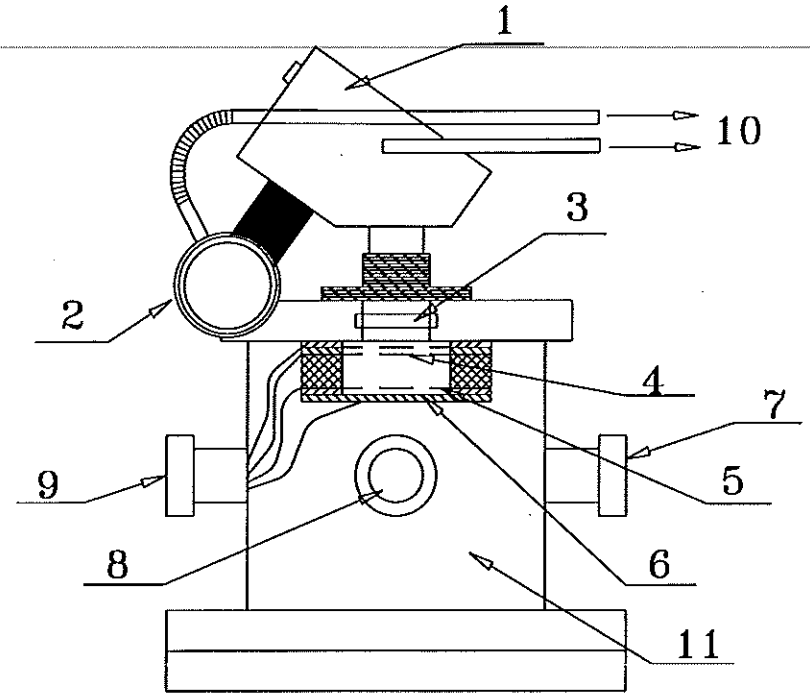

1. Monochromator;
2. Hydrogen lamp;
3. UV window;
4. Mesh;
5. Anode mesh;
6. Photocathode;
7. Vacuum port;
8. Gas port;
9. Signal & H.V. port;
10. To nitrogen gas bottle;
11. S.S. vacuum chamber.

Figure 1: The test chamber for measurement of the quantum efficiency of CsI photocathodes in a parallel-plate avalanche chamber operated with various gases.

studies near 170-nm wavelength, the cutoff of UV-grade quartz, all light paths must be in nitrogen. The chamber was be pumped down with a Balzers TSH180 oil-free molecular-drag/diaphragm pump system to 5×10^{-5} Torr. The chamber was baked at 60°C every night between data runs, and the photocathode could also be heated to 60°C by a flexible Kapton heating pad (Omegalux KHLV101-10) attached to the back side of the photocathode. Data were taken only after a few days of baking at which time the moisture level inside the chamber was less than 1 ppm, the lower limit of sensitivity of our Kahn Cermet hygrometer. All of the hydrocarbon gases used in this study were scientific grade (MG Industries) with minimum purity was: methane 99.9995%, ethane 99.95%, isobutane 99.96%, and helium 99.999%. The hydrocarbon gas was admitted to the chamber through Oxisorb (MG Industries); according to manufacturer's specification the discharge gas purity should be < 0.1 ppm O_2 and < 0.5 ppm H_2O when used with scientific-grade gases.

For measurement of the relative quantum efficiency of the CsI photocathode, it was held at negative high voltage and the anode mesh was grounded as shown in Fig. 2(a).

gas. Photoelectrons produced in the transfer region did not produce avalanches in this configuration. A correction was made for the substantial attenuation of the UV light in the transfer region, thereby deriving the quantum efficiency for CsI+TMAE cathodes also reported in Fig. 3.

2.2 Effect of Different Gases on the Quantum Efficiency

We have used the apparatus described above to measure the quantum efficiency for three different gases: methane, ethane and isobutane. The results are summarized in Fig. 3.

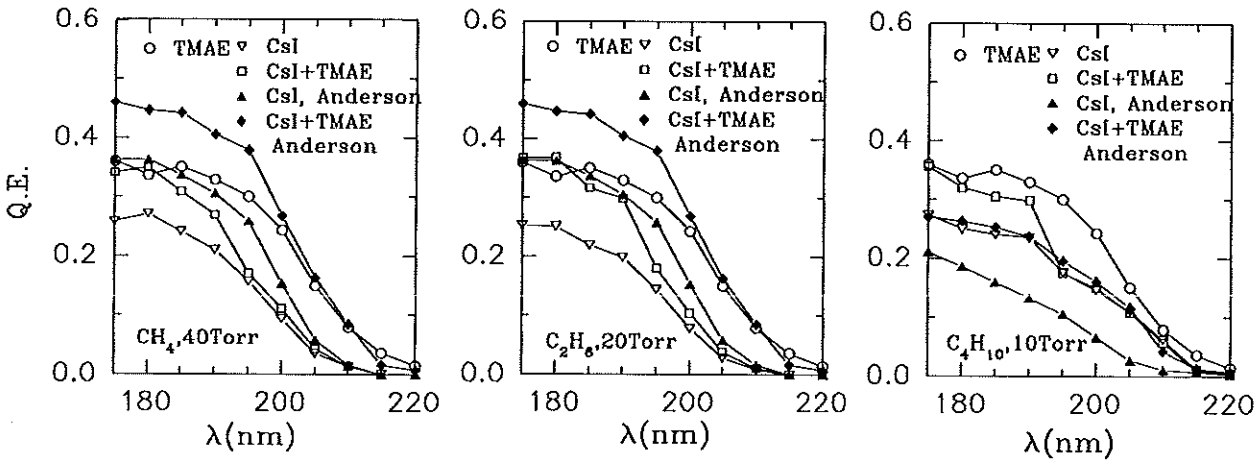

Figure 3: The quantum efficiency of CsI (a) in CH_4, (b) in C_2H_6, and (c) in C_4H_{10}. Also shown are data points from Anderson *et al.* [14].

We do not find as big a difference between the quantum efficiency for CH_4 and C_4H_{10} as reported by Anderson *et al.* [14]; the quantum efficiency of our photocathode in CH_4 is lower than theirs, while in C_4H_{10} it is higher than theirs. The thickness of our photocathode was 5000 Å.

2.3 Effect of Water Vapor on the Quantum Efficiency

Because of the large band gap of CsI (≈ 6 V), it is believed that CsI photocathodes do not oxidize on exposure to air. The observed reduction of the quantum efficiency on exposure to air is mainly blamed on the effect of water vapor.

We studied this effect by exposing the chamber to a controlled amount of water vapor for 15 minutes. Then we pumped down the chamber, filled it with the working gas, and measured the quantum efficiency. Next, the whole chamber was heated up to 60° with an infrared lamp; the photocathode could also be heated by a heating pad mounted on the back of the photocathode plate. After various intervals the chamber was reactivated with gas and the quantum-efficiency measurement repeated. The recovery of the quantum efficiency *vs.* time of heating is shown in Fig. 4.

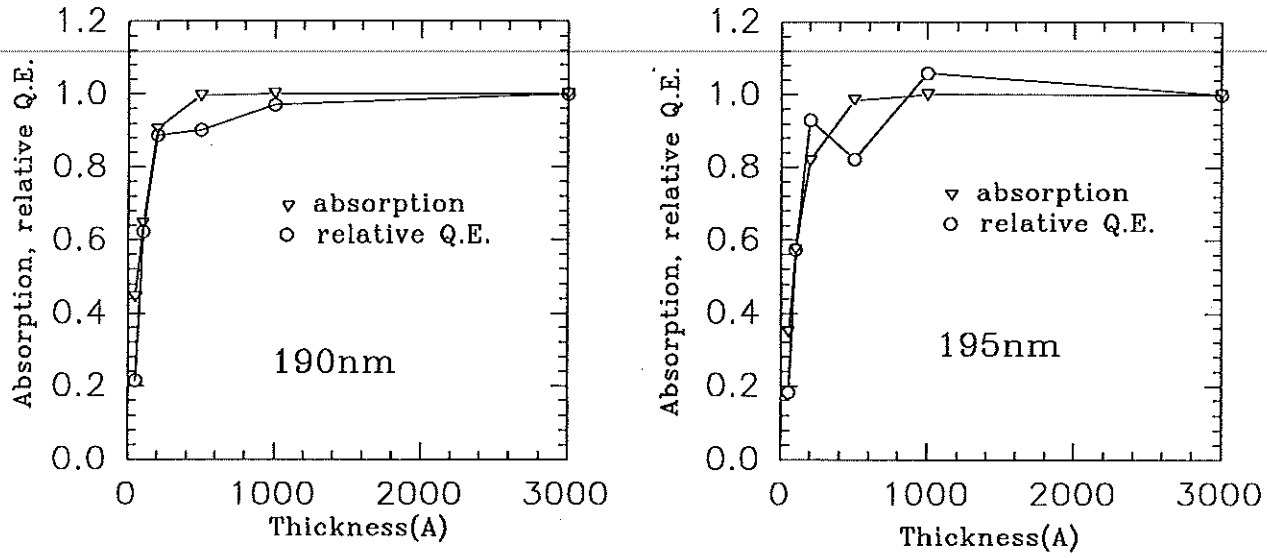

Figure 5: The UV absorption and quantum efficiency of CsI films *vs.* film thickness (a) at 190 nm, and (b) at 195 nm.

2.5 Effect of the Density of CsI Film on the Quantum Efficiency

During studies in the early 1960's low-density KCl films showed enhanced secondary emission [19, 21]. Interpretations were given that the internal electric field in a 'fluffy' film might enhance the secondary emission, and/or that the transport of the secondary electrons is more favorable than in normal-density films.

We have studied several 'fluffy' films in our lab. For full-density CsI films the secondary emission ratio was observed to be $\sim$ 20 (as reported by many others). With a low-density CsI film (5% of normal density) the secondary emission ratio was observed to be as high as 100. Details of this work are beyond the scope of this paper.

An immediate question is whether 'fluffy' CsI films would show enhanced photoemission? To answer this we made a low-density CsI film of 1000-Å effective thickness (*i.e.*, the same area density a a normal film of that thickness). Instead of performing the CsI evaporation under good vacuum, we filled the bell jar with $\sim$ 10 mTorr Ar. The 'fluffy' film was deposited in two minutes at the rate of $\sim$ 4 to 10 Å/sec. The CsI film was examined under a microscope, and the thickness estimated to be 20 times that of a 0.1-μm full-density film; *i.e.*, the density was $\approx$ 5% of normal.

The measured quantum efficiencies 1000-Å high-and low-density CsI photocathodes are summarized in Fig. 6. The quantum efficiency of the low-density CsI film was only $\sim$ 80% of high-density one. Certainly more carefully studies need to be done before drawing definitive conclusions about low-density photocathodes.

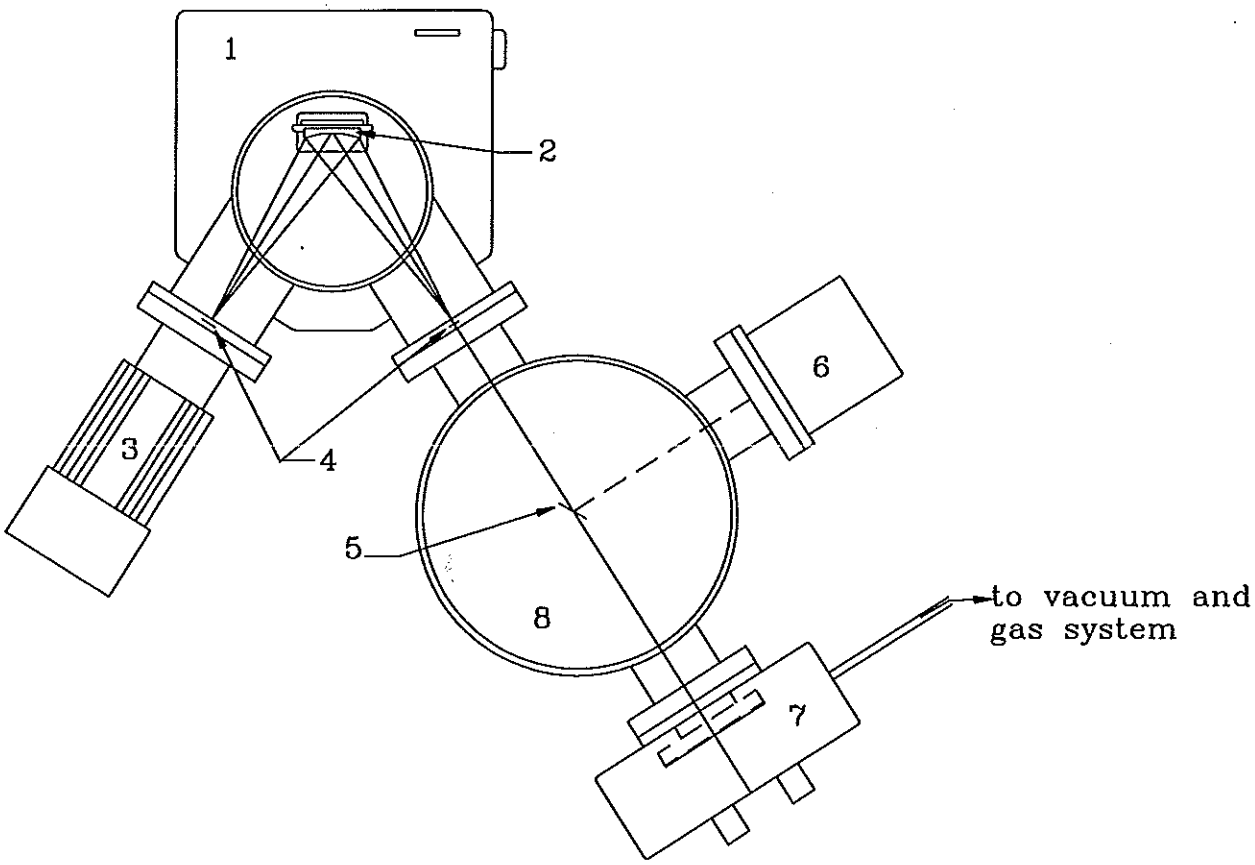

1, Model 234/302 0.2m vacuum monochromator;
2, Holographic grating;
3, Model 632 deuterium source unit;
4, Entrance and exit slits;
5, UV mirror;
6, Model 654 side-on PMT detector with sodium salicylate screen;
7, Test chamber(semi-transparent or reflective photocathode).
8, Vacuum compatible sample chamber.

Figure 7: Sketch of the VUV monochromator.

3.1 Transmittance of CsI Films

We measured the transmittance of 51-, 100- and 310-Å-thick CsI coatings evaporated onto thin LiF windows, with results summarized in Fig. 9(a). The absorption lengths of CsI coatings deduced from those transmittance curves are shown in Fig. 9(b) and are reasonably consistent. For CsI photocathodes used with quartz windows the wavelength region of interest is 165 to 220 nm, over which the absorption length varies between 100 and 200 Å.

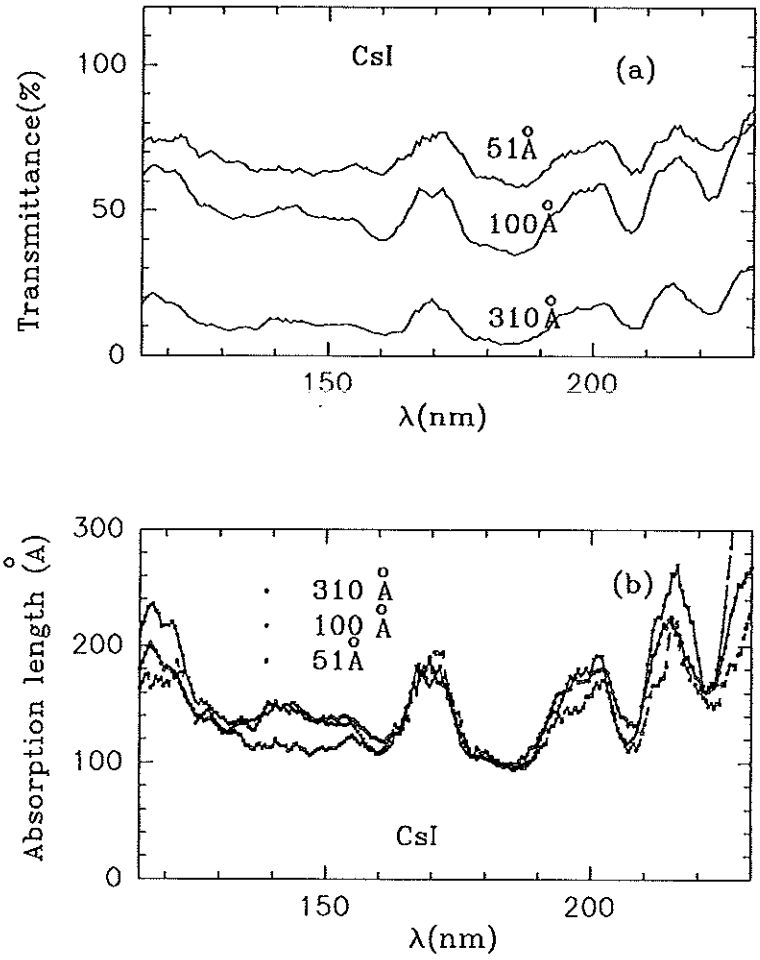

Figure 9: The transmittance curves of three CsI coatings: (a) Transmittance, (b) Absorption length.

We also compared the transmittance of a freshly made CsI film and that of the same one after exposure to air for 14 hours. As seen in Fig. 10 the transmittance was reduced by $\sim$ 10% after 14 hours.

measured for the empty cell. Because of the adsorption of TMAE on the surface of the MgF_2 windows, the second spectrum was quite different from one taken before admitting TMAE vapor. We used the last spectrum as the reference when calculating the TMAE absorbance, which is defined as $A = \log_{10}(1/T)$, where T is the transmittance.

To compare our results with previous work, we also calculated the extinction coefficient ϵ, which is related to the absorbance by $A = \epsilon cl$, where c is the gas concentration in moles per liter and l is the length of the gas sample. The results are shown in Fig. 11, along with results from other authors' [18, 23]. The general shape of our curve is similar to the others, but our values are generally lower. A big discrepancy between our data and that of Holroyd *et al.* is seen below 140 nm where their curve increases sharply. No data are available below 150 nm from Bräuning *et al.*

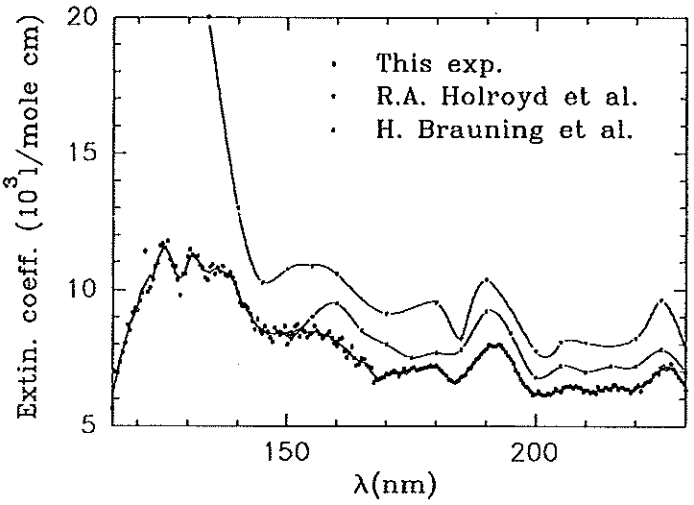

Figure 11: The extinction coefficient of the TMAE.

3.3 The Transmittance of Thin Metal Films

To prepare semitransparent CsI photocathodes we need a good UV-transparent conductive thin metal film as a substrate. We investigated three metals, tungsten, nickel and chromium, which are presently used for this purpose in industry. Thin films were evaporated onto quartz windows either with an electron gun (tungsten), or with a heated boat (nickel and chromium). Transmittance measurements are shown in Fig. 12(a) taken with a Perkin-Elmer model $\lambda 3$ spectrophotometer, which is limited to wavelengths longer than 190 nm.

For our studies of semitransparent photocathodes we used a 66-Å-thick Cr film, and measured it transmittance with a VUV monochromator with results as shown in Fig. 12(b). The lower bound of the spectrum was set at 165 nm by the transmittance of quartz windows.

The resistivities of those film were measured with an Alessi C4S four-point probe [24]. Only the Cr films show promising results: $\rho_s = 0.3 M\Omega/\square$ for 21-Å Cr, $\rho_s = 0.08 M\Omega/\square$ for 54-Å Cr. For other two films the resistivities were too large to determine measurable with this set-up.

4 Investigations of Semitransparent CsI Photocathodes

4.1 Experimental Set-up

The experimental set-up employed in this investigation is sketched in Fig. 7 and details of the chamber are shown in Fig. 13. One surface of a half-inch-thick quartz window was coated with a 66-Å-thick Cr film. Around with the periphery of the surface a 0.25-inch-wide Al ring (1000Å thick) was evaporated on the top of Cr film. The rest of the surface area was evaporated with CsI.

The cathode was separated from the anode by a 1.6-mm-thick copper-clad G-10 ring, to the other side of which was soldered an 80-% transparent stainless-steel mesh. By tightly compressing this ring together with the coated side of the window, a PPAC with CsI coating as photocathode and the mesh as anode was formed. A similar chamber with two meshes and a reflective photocathode was also constructed, with an electrode arrangement as shown in Figs. 1 and 2. As a reference for the measurement of the quantum efficiency of the semitransparent photocathode in the first chamber, the second chamber was filled with TMAE vapor, following the procedures discussed in sec. 2 above.

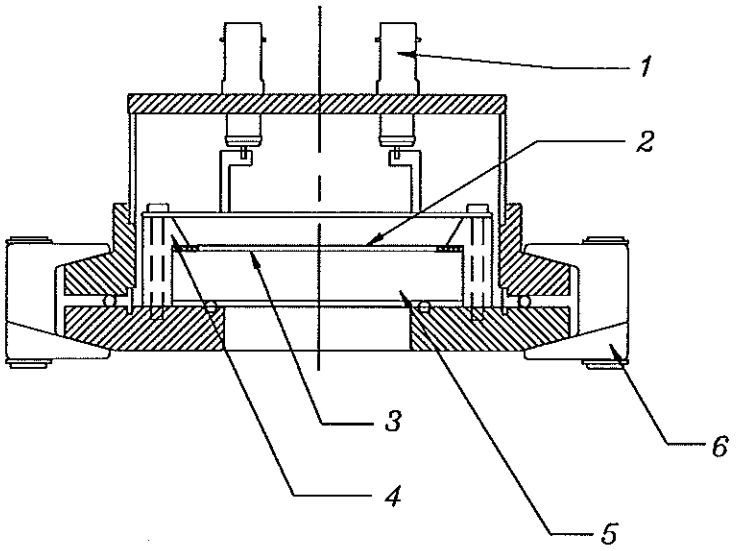

1, SHV connectors;
2, Mesh as anode;
3, Cr coated surface;
4, Teflon clamp;
5, Quartz window, 3" diameter, 0.5" thick;
6, Chain clamp.

Figure 13: The semitransparent-photocathode test chamber.

The UV mirror at the center of the sampling chamber (Fig. 7) could be inserted to deflect the light to the side port, or removed to permit light to exit the front port. A PMT detector

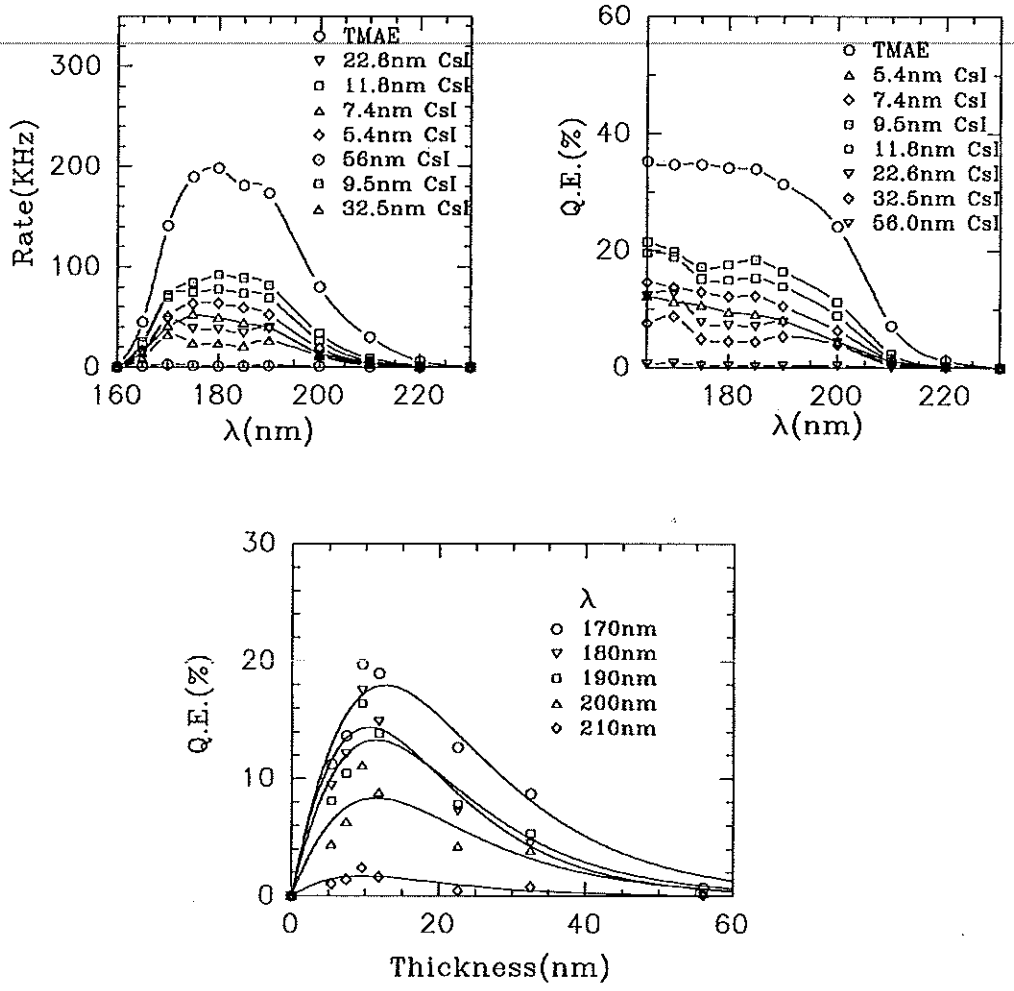

Figure 14: The quantum efficiency of semitransparent CsI photocathodes: (a) Event rate *vs.* wavelength for TMAE vapor and seven CsI films, (b) quantum efficiency *vs.* wavelength for TMAE vapor (from [18]) and seven CsI films, (c) quantum efficiency *vs.* CsI thickness at five wavelengths. wavelength.

4.4 Transmittance of Moisturized CsI Films

When we finished the quantum-efficiency measurement for each semitransparent CsI photocathode, the absorbance of the CsI-coated window was measured immediately with a Perkin-Elmer $\lambda 3$ spectrophotometer. The absorbance curves are shown in Fig. 16. If the CsI film was exposed to an extremely humid atmosphere (such as the breath of a human being), the appearance of the film turned milky immediately, and the UV absorbance of the film was destroyed completely (*i.e.*, it became transparent to UV light). Measurements of the absorbance of several highly moisturized CsI films are shown in Fig. 17. According to our preliminary observation, once the films became UV transparent due to moisture, their former absorbance could not be restored by heating. This is in contrast to the results of sec. 2.3 for films exposed to $\leq 100\%$ humidity.

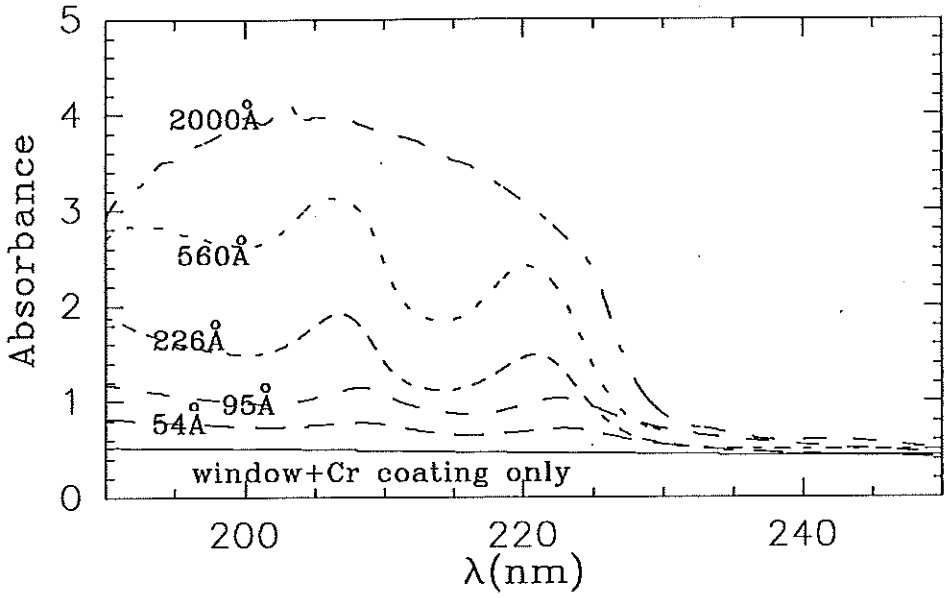

Figure 16: The absorbance of semitransparent CsI films.

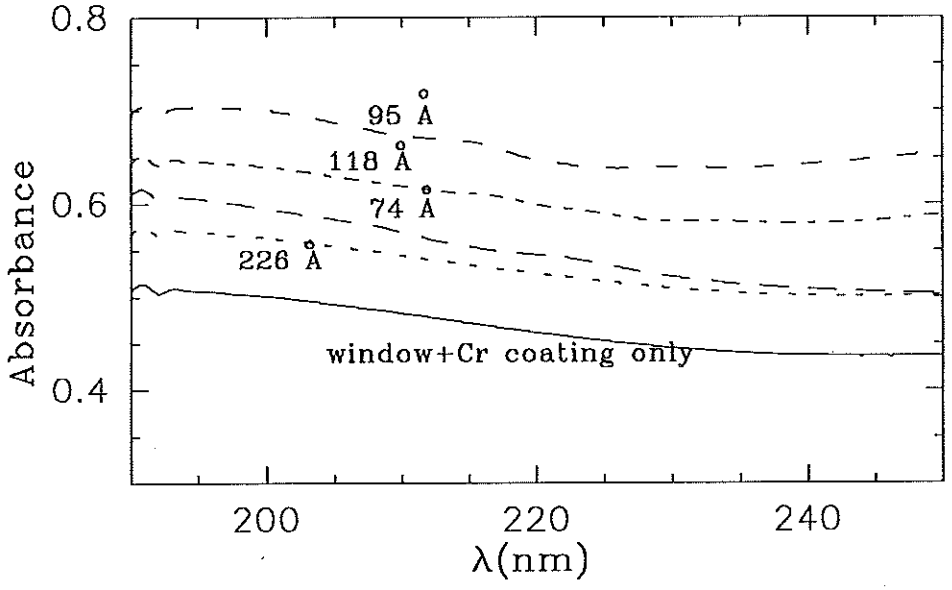

Figure 17: The absorbance of highly moisturized CsI films. They are largely transparent to UV light.

A more sophisticated model based on the diffusion equation can be used to describe the transport process of photo-electron in the CsI film (see the Appendix). In this the expression for the observed quantum efficiency of a semitransparent photocathodes becomes

$$\text{Q.E.}_{\text{obs}} = \frac{QTL}{2\sinh\frac{d}{L}}\left(\frac{1-e^{d/L-d/\lambda}}{L-\lambda} - \frac{1-e^{-d/L-d/\lambda}}{L+\lambda}\right), \qquad \text{(semitransparent)}.$$

The parameters fitted to the data of Fig. 14 with the diffusion model are summarized in Fig. 18 along with the escape length taken from a Monte Carlo calculation by Akkerman *et al.* [15]. In this model an electron that reaches the interface between the CsI and metal films will be captured by the metal film immediately.

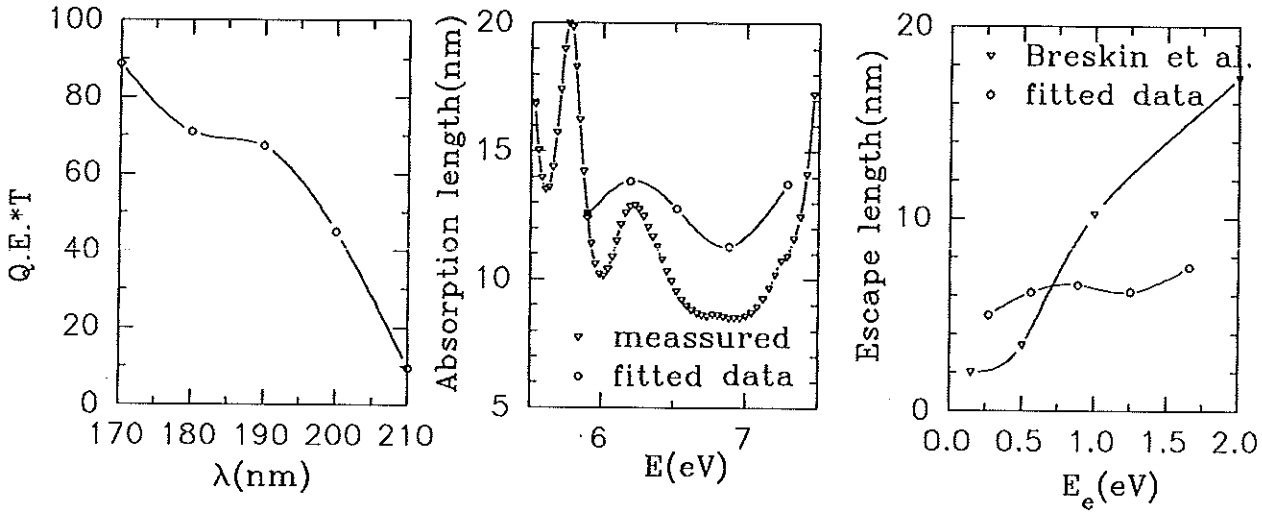

Figure 18: Results of fitting the observed quantum efficiency of semitransparent CsI photocathodes to a diffusion model. The UV photon energy is labelled as E. The photoelectron energy E_e is measured with respect to the vacuum level, so $E_e = E - \phi$ where the work function $\phi \approx 5.6$ V corresponds to about 220 nm. The 'measured' optical absorption length for CsI is taken from Fig. 9.

According to the diffusion-model fits the values of QT are very high. Recall that Q is the intrinsic quantum efficiency that a photon absorbed in CsI produces an electron that moves away from the photoabsorption site. Because of the short escape length in CsI the observed quantum efficiency is considerably lower than the intrinsic quantum efficiency. Of course, QT cannot exceed unity.

Many groups have measured the quantum efficiency of CsI to be close to that of TMAE vapor. But for TMAE vapor there is no electron escape problem; once a photoelectron leaves TMAE molecule it has a high probability of being observed. Hence we infer that the intrinsic quantum efficiency of CsI is actually much higher than that of TMAE vapor.

We also can calculate the quantum efficiency of reflective CsI films, and the simple model predicts

$$\text{Q.E.}_{\text{obs}} = QT\frac{L}{L+\lambda}\left(1-e^{-d(L+\lambda)/L\lambda}\right), \qquad \text{(reflective)},$$

quantum efficiency observed with a flat surface is only 0.33 of the intrinsic quantum efficiency, but with the wedge-shaped photocathode it would rise to 0.38, a 15% improvement.

When a CsI photocathode is used to detect Čerenkov light from a liquid or solid radiator, the light will have non-normal incidence. This automatically improves the quantum efficiency compared to that inferred from studies with normally incident light. Hence we have one more indication of how well suited CsI photocathodes are for use in RICH detectors.

5 Appendix. Models of Electron Transport in CsI Films

We review several models of electron transport in CsI photocathodes.

For very thick films it nearly suffices to characterize the transport by a single 'escape length' that we will call L in this note. For thin films more care is needed. An interesting issue is whether electrons that are produced heading away from the surface scatter enough to eventually reverse direction and escape. Also, when semitransparent photocathodes are used the performance is very sensitive to electron transport.

We label **reflective** photocathodes as those for which the signal electrons are collected from the same surface across which the photons enter, and **semitransparent** cathode films as those for which photons enter one surface and electrons are collected from the other.

Accurate modelling of electron transport is based on the Boltzmann transport equation, along with characterization of the various scattering cross sections. However, no analytic solutions are available in this approach, which must be pursued by Monte Carlo calculations. Here we review three one-dimensional models of increasing sophistication:

1. A simple exponential model.
2. A simple diffusion model.
3. A more intricate diffusion model.

The third model may have sufficient accuracy for the present state of studies of CsI photocathodes for RICH detectors.

5.1 An Exponential Model

In this model we suppose that an electron which is photoejected at a distance x from the surface has probability of escape

$$G(x) = Te^{-x/L}. \tag{1}$$

We label this probability as G as it is a kind of Green's function for the electron transport. In this, T is the probability that if the electron reaches the surfaces it actually escapes. As CsI has a low electron affinity ($\approx$ 0.1 eV) it is expected that $T \approx 1$. Parameter L is the escape length, which is finite because electrons might be trapped on defects, or more likely just lose energy until they can no longer escape.

We close this section with the qualitative observation that since the yield of semitransparent cathodes depends on the difference between the escape length L and the optical absorption length λ while that of reflective cathodes depends on the sum, the former is much more sensitive to the details of electron transport.

5.2 A Diffusion Model

A tacit assumption of the exponential model was that the electron transport is the average effect of a a large number of nearly elastic collisions. The resulting random walk should be well described as a diffusion process so long as the number of collisions is indeed very large.

The first form of diffusion model that we consider is one articulated by Chen *et al.* [25]. The one-dimensional density of electrons $\rho(x,t)$ is subject to lossless diffusion described by a diffusion coefficient D. That is, the flux of electrons across the surface $x =$ constant is

$$j = -D\frac{\partial \rho}{\partial x}. \tag{8}$$

Combining this with the equation of continuity,

$$\frac{\partial \rho}{\partial t} = -\frac{\partial \rho}{\partial x}, \tag{9}$$

we arrive at the lossless diffusion equation

$$\frac{\partial \rho}{\partial t} = D\frac{\partial^2 \rho}{\partial x^2}. \tag{10}$$

Loss of electrons is simply modelled by a decay constant τ according to

$$\frac{\partial \rho}{\partial t} = -\frac{\rho}{\tau}. \tag{11}$$

Combining eqs. (10) and (11) we arrive at the lossy diffusion equation:

$$\frac{\partial \rho}{\partial t} = D\frac{\partial^2 \rho}{\partial x^2} - \frac{\rho}{\tau}. \tag{12}$$

For boundary conditions we suppose that the surfaces at $x = 0$ and $x = d$ of the photocathode are perfect sinks (transmission coefficient $T = 1$), so that

$$\rho(0,t) = 0 = \rho(d,t). \tag{13}$$

For the initial condition that a single electron is created at x_0 at $t = 0$ we have

$$\rho(x_0,0) = \delta(x_0). \tag{14}$$

The diffusion equation (12) then has the solution

$$\rho(x,t) = \frac{2}{d}e^{-t/\tau}\sum_n \sin\frac{n\pi x_0}{d}\sin\frac{n\pi x}{d}e^{-Dn^2\pi^2 t/d^2}. \tag{15}$$

5.3 The Diffusion Model of Kane

A generalization of the diffusion model has been given by Kane [27]. See also ref. [28].

In this model we include a scattering length

$$\lambda_{ep} \text{ for electron-phonon interactions,} \tag{23}$$

and another scattering length

$$\lambda_{ee} \text{ for electron-electron interactions.} \tag{24}$$

An important assumption of the model is that if an electron suffers a collision with another electron it loses so much energy that it can no longer escape. On the other hand, the electron-phonon collisions are taken to be elastic.

Then an electron produced at depth x has probability

$$P_0(x) = \frac{T}{2} e^{-x/\lambda_e} \tag{25}$$

of reaching the surface with zero scatters along the way and then escaping. In this, λ_e is the combined scattering length

$$\frac{1}{\lambda_e} = \frac{1}{\lambda_{ep}} + \frac{1}{\lambda_{ee}}. \tag{26}$$

As before, T is the surface-transmission coefficient. The factor $1/2$ in eq. (25) occurs because an electron can reach the surface with zero scatters only if it is heading towards the surface initially.

The total probability $G(x)$ that an electron produced at x escapes from the surface at $x = 0$ is taken at the sum over the probabilities that it escapes with exactly n electron-phonon scatters along the way:

$$G(x) = \sum_n P_n(x). \tag{27}$$

(To escape, an electron must always have zero electron-electron scatters.) Each probability $P_n(x)$ can be obtained from $P_{n-1}(x)$ by the integral equation

$$P_n(x) = \int_0^x P_{n-1}(y) e^{-(x-y)/\lambda_e} \frac{dy}{2\lambda_{ep}} + \int_x^d P_{n-1}(y) e^{-(y-x)/\lambda_e} \frac{dy}{2\lambda_{ep}}. \tag{28}$$

In this the electron is produced at x and drifts to y where it suffers its first electron-phonon collision in the interval dy. It then reaches the surface after $n-1$ additional electron-phonon collisions with probability $P_{n-1}(y)$. The two terms arise according to the initial direction of the electron.

Kane [27] notes that in principle there should be additional terms in eq. (28) corresponding to the cases that the electron reaches a surface and bounces off before suffering its first electron-phonon collision. We ignore these terms, which are important only for extremely thin films.

By summing eq. (28) from $n = 1$ to ∞ and adding $P_0(x)$ we obtain an integral equation for $G(x)$:

$$G(x) = \frac{1}{2\lambda_{ep}} \left(\int_0^x G(y) e^{-(x-y)/\lambda_e} dy + \int_x^d G(y) e^{-(y-x)/\lambda_e} dy \right) + P_0(x). \tag{29}$$

We now find that

$$G(x) = T\frac{\sinh\frac{d-x}{L} + Ce^{(d-x)/L}}{\sinh\frac{d}{L} + C(e^{d/L} + \cosh\frac{d}{L})}. \tag{40}$$

We see that as parameter C goes to zero we recover the previous diffusion model. For thick cathodes the escape probability goes to

$$G(x) = Te^{-x/L}(1-C), \qquad (d \gg L), \tag{41}$$

and for thin cathodes

$$G(x) = T\frac{\frac{d-x}{L} + C}{\frac{d}{L} + 2C}, \qquad (d \ll L). \tag{42}$$

In this model, if d/L becomes less than C we note that $G(x) \to T/2$. Since $\lambda_e \approx CL$, this limit corresponds to $d < \lambda_e$ and so the electrons reach the surface without scattering, which implies the escape probability should be just $T/2$. Hence the diffusion model of Kane has better behavior for very thin cathodes that does the first diffusion model.

We complete our discussion of this model by calculating the yields for reflective and semitransparent cathodes:

$$Y_R = \frac{QL}{2[\sinh\frac{d}{L} + C(e^{d/L} + \cosh\frac{d}{L})]}\left((1+2C)\frac{e^{d/L} - e^{-d/\lambda}}{L+\lambda} - \frac{e^{-d/L} - e^{-d/\lambda}}{L-\lambda}\right), \tag{43}$$

and

$$Y_S = \frac{QL}{2[\sinh\frac{d}{L} + C(e^{d/L} + \cosh\frac{d}{L})]}\left((1+2C)\frac{1 - e^{d/L-d/\lambda}}{L-\lambda} - \frac{1 - e^{-d/L-d/\lambda}}{L+\lambda}\right). \tag{44}$$

6 References

[1] J. Séguinot and T. Ypsilantis, *Photo-ionization and Čerenkov Ring Imaging*, Nucl. Instr. and Meth. **142** (1977) 377.

[2] V. Peskov *et al.*, *Liquid and Solid Organic Photocathodes*, Nucl. Instr. and Meth. **A269** (1988) 149.

[3] V. Dangendorf *et al.*, *A Gas-Filled UV-Photon Detector with CsI Photocathode for the Detection of Xe Light*, Nucl. Instr. and Meth. **A289** (1990) 322.

[4] J. Séguinot *et al.*, *Reflective UV Photocathode with Gas-Phase Electron Extraction: Solid, Liquid, and Adsorbed Thin Films*, Nucl. Instr. and Meth. **A297** (1990) 133.

[5] B. Hoeneisen, D.F. Anderson and S. Kwan, *A CsI-TMAE Photocathode with Low-Pressure Readout for RICH*, Nucl. Instr. and Meth. **A302** (1991) 447.

[6] G. Charpak *et al.*, *Investigation of Operation of a Parallel-Plate Avalanche Chamber with a CsI Photocathode Under High Gain Conditions*, Nucl. Instr. and Meth. **A307** (1991) 63.

[7] V. Dangendorf *et al.*, *Progress in Ultrafast CsI-Photocathode Gaseous Imaging Photomultipliers*, Nucl. Instr. and Meth. **A308** (1991) 519.

[25] D.M. Chen *et al.*, *Measurement of Positron Reemission from Thin Single-Crystal W(100) Films*, Phys. Rev. B **31** (1985) 4123.

[26] J. Llacer and E.L. Garwin, *Electron-Phonon Interaction in Alkali Halides. I. The Transport of Secondary Electrons with Energies between 0.25 and 7.5 eV*, J. Appl. Phys. **40** (1969) 2766.

[27] E.O. Kane, *Simple Model for Collision Effects in Photoemission*, Phys. Rev. **147** (1966) 335.

[28] B.L. Henke, J.P. Knauer and K. Premaratne, *the Characterization of X-Ray Photocathodes in the 0.1-10-keV Photon Energy Region*, J. Appl. Phys. **52** (1981) 1509.